

# *Drosophila* patterning is established by differential association of mRNAs with P bodies

Timothy T. Weil<sup>1,5</sup>, Richard M. Parton<sup>1,5</sup>, Bram Herpers<sup>2,6</sup>, Jan Soetaert<sup>1,6</sup>, Tineke Veenendaal<sup>3</sup>, Despina Xanthakis<sup>2,3</sup>, Ian M. Dobbie<sup>1</sup>, James M. Halstead<sup>1</sup>, Rippei Hayashi<sup>4</sup>, Catherine Rabouille<sup>2,3,7</sup> and Ilan Davis<sup>1,7</sup>

The primary embryonic axes in flies, frogs and fish are formed through translational regulation of localized transcripts before fertilization<sup>1</sup>. In *Drosophila melanogaster*, the axes are established through the transport and translational regulation of *gurken* (*grk*) and *bicoid* (*bcd*) messenger RNA in the oocyte and embryo<sup>1</sup>. Both transcripts are translationally silent while being localized within the oocyte along microtubules by cytoplasmic dynein<sup>1–4</sup>. Once localized, *grk* is translated at the dorsoanterior of the oocyte to send a TGF- $\alpha$  signal to the overlying somatic cells<sup>5</sup>. In contrast, *bcd* is translationally repressed in the oocyte until its activation in early embryos when it forms an anteroposterior morphogenetic gradient<sup>6</sup>. How this differential translational regulation is achieved is not fully understood. Here, we address this question using ultrastructural analysis, super-resolution microscopy and live-cell imaging. We show that *grk* and *bcd* ribonucleoprotein (RNP) complexes associate with electron-dense bodies that lack ribosomes and contain translational repressors. These properties are characteristic of processing bodies (P bodies), which are considered to be regions of cytoplasm where decisions are made on the translation and degradation of mRNA. Endogenous *grk* mRNA forms dynamic RNP particles that become docked and translated at the periphery of P bodies, where we show that the translational activator Oo18 RNA-binding protein (Orb, a homologue of CEPB) and the anchoring factor Squid (Sqd) are also enriched. In contrast, an excess of *grk* mRNA becomes localized inside the P bodies, where endogenous *bcd* mRNA is localized and translationally repressed. Interestingly, *bcd* mRNA dissociates from P bodies in embryos following egg activation, when it is known to become translationally active. We propose a general principle

of translational regulation during axis specification involving remodelling of transport RNPs and dynamic partitioning of different transcripts between the translationally active edge of P bodies and their silent core.

At the dorsoanterior corner of the oocyte, localized *grk* mRNA is associated with electron-dense structures<sup>7</sup>, which were originally characterized in nurse cells<sup>8</sup> and later in the oocyte as sponge bodies<sup>7</sup>. These structures have subsequently been shown to share at least some components with yeast and mammalian P bodies<sup>9–11</sup>. We, therefore, refer to sponge bodies as P bodies. To investigate whether, like *grk*, *bcd* mRNA is associated with P bodies, we used *in situ* hybridization (ISH) with an antisense *bcd* probe combined with immuno-electron microscopy (IEM) on frozen sections<sup>12</sup>. We found that *bcd* mRNA is also associated with P bodies in mid-oogenesis (Fig. 1a and Supplementary Fig. S1). Closer examination revealed that *grk* mRNA is present along the periphery of the P body (Fig. 1b,c), whereas *bcd* is mostly present within its interior (Fig. 1a,c). To characterize this further, we co-visualized endogenous *grk* mRNA and a DEAD-box helicase Maternal expression at 31B (Me31B), a well-established P body marker<sup>13</sup>. We found that *grk* mRNA localizes outside a core zone of concentrated Me31B labelling (Fig. 1d). We then performed a quantitative analysis of the density of gold as a function of the distance from the border of the P body. This analysis applied to Me31B and Orb (Supplementary Fig. S2a–b' and Methods) shows that P bodies are organized into two different regions: a core containing most of the Me31B and an edge, the outermost 60–80 nm of electron-dense material, defined as 70 nm for the convenience of analysis (Fig. 1e and Supplementary Fig. S2c). We found that, relative to the surrounding cytoplasm, *grk* mRNA is 23 times more concentrated at the edge of the P body whereas *bcd* is sixfold more concentrated in the P body core (Fig. 1e).

<sup>1</sup>Department of Biochemistry, The University of Oxford, South Parks Road, Oxford OX1 3QU, UK. <sup>2</sup>Department of Cell Biology, UMC Utrecht, Heidelberglaan 100, 3584 CX Utrecht, The Netherlands. <sup>3</sup>Hubrecht Institute for Stem Cell Research and Developmental Biology, Uppsalalaan 8, 3584 CT Utrecht, The Netherlands.

<sup>4</sup>London Research Institute, Cancer Research UK, 44 Lincoln's Inn Fields, London WC2A 3LY, UK. <sup>5</sup>Joint first authors. <sup>6</sup>Present addresses: Division of Toxicology Leiden University Einsteinweg 55, 2300 RA Leiden, The Netherlands (B.H.); Centre for Neuroregeneration, Chancellors Building, 49 Little France Crescent, Edinburgh EH16 4SB, UK (J.S.).

<sup>7</sup>Correspondence should be addressed to C.R. or I.D. (e-mail: c.rabouille@hubrecht.eu or ilan.davis@bioch.ox.ac.uk)

Received 8 February 2012; accepted 22 October 2012; published online 25 November 2012; DOI: 10.1038/ncb2627

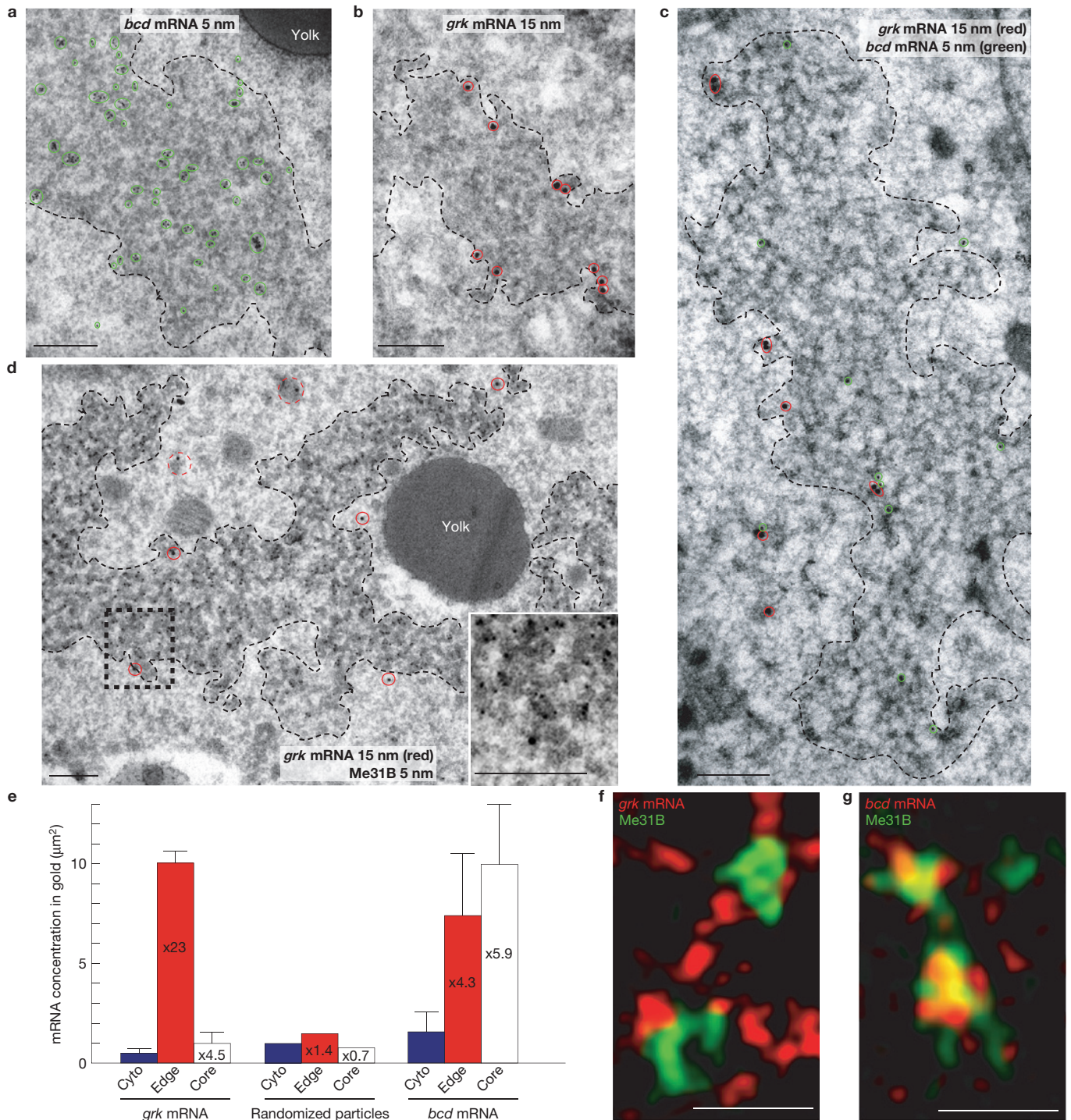


**Figure 1** Differential association of *bcd* and *grk* with P bodies. (a–d) mRNA detection at the dorsoanterior corner (for orientation, see Fig. 2a) by ISH–IEM on wild-type ultrathin frozen sections of stage-9 oocytes; P bodies are marked with a dashed black line. (a) *bcd* mRNA (5 nm, green circles) is present both inside and at the edge of electron-dense P bodies. Gold particles here cluster owing to the use of a bridging antibody. (b) *grk* mRNA (15 nm, red circles) is enriched at the edge of P bodies. (c) *bcd* mRNA (5 nm, green circles) and *grk* mRNA (15 nm, red circles) can associate with the same P body but *bcd* is enriched inside. (d) *grk* mRNA (15 nm, red circles) docks at the edge of the P body (black dashed rectangle magnified, inset bottom right), just outside the Me31B-dense core region (5 nm gold), whereas *grk* transport particles, as described

previously<sup>7</sup>, are detected in the cytoplasm at a short distance from the P body (15 nm, red dashed circles). (e) mRNA density (gold  $\mu\text{m}^{-2}$ ) in the P body sub-regions when compared with the surrounding cytoplasm. For comparison, randomized particles were analysed in an identical way to RNAs. Error bars show s.e.m. of gold density per scan (*grk*  $n = 13$ , *bcd*  $n = 11$ ). (f, g) Fixed stage-8/9 Me31B::GFP-expressing oocytes imaged using the OMX structured illumination super-resolution mode (3D-SIM) with double labelling of either *grk*<sup>+</sup> mCherry (f), which mainly interdigitates with Me31B (green) while showing some co-localization at the edge (yellow), or *bcd*<sup>+</sup> RFP *grk* mRNA (red; g), which shows significant co-localization (yellow) with Me31B (green). Scale bars, 200 nm (a–d); 0.5  $\mu\text{m}$  (f, g).

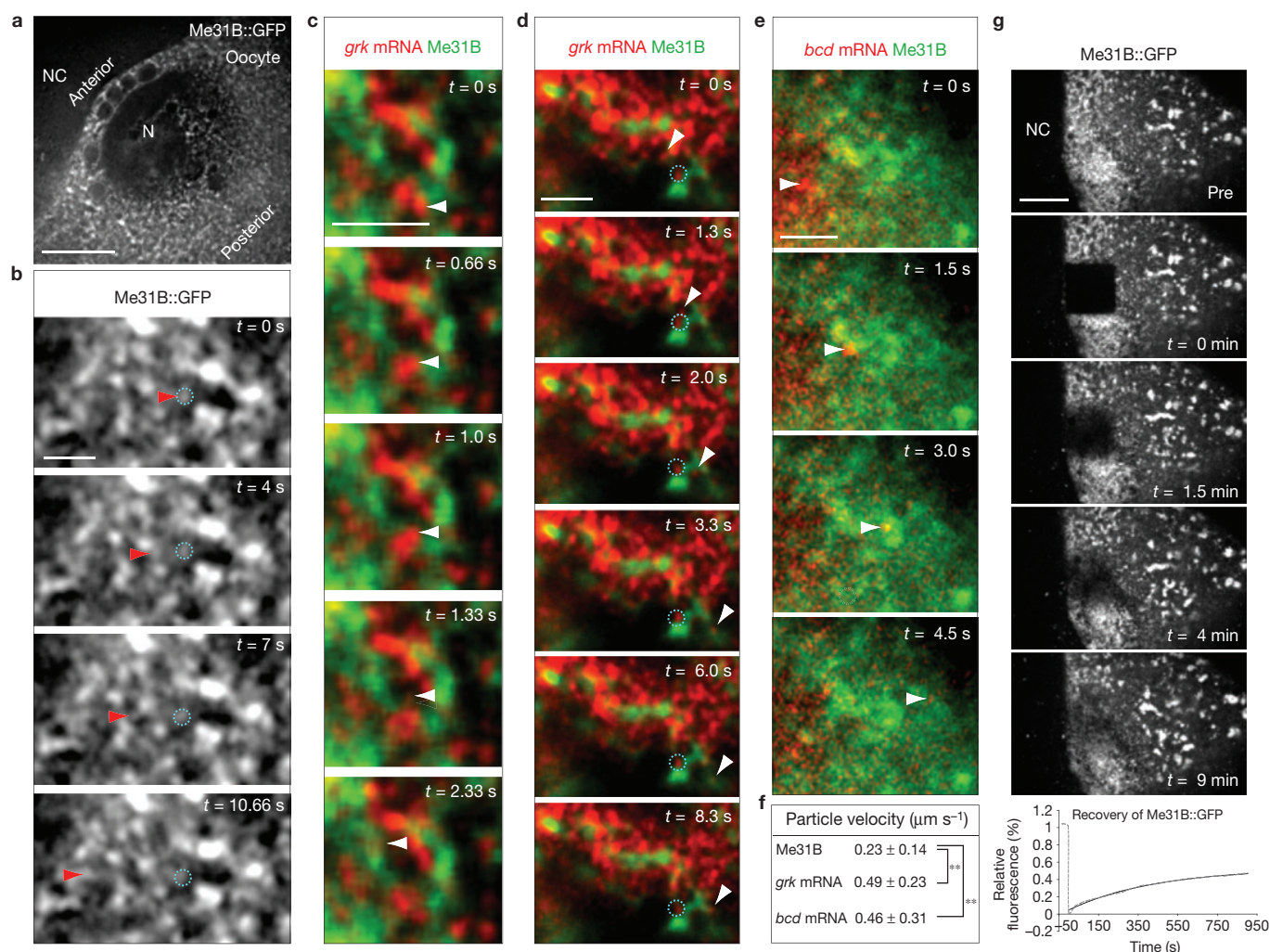


**Figure 2** Dynamics of *grk*, *bcd* and Me31B particles in live oocytes. (a) Low-magnification wide-field image of the dorsoanterior corner of a stage-8/9 egg chamber expressing Me31B::GFP. (b) Me31B::GFP-expressing oocytes show small faint dynamic particles of Me31B (red arrowheads) moving between and fusing together with other often larger, bright and static (dashed cyan circles) Me31B bodies (Supplementary Movies S1 and S2). (c,d) *grk*\**mCherry*- and Me31B::GFP-expressing oocytes show *grk* mRNA particles (white arrowheads) moving independently of Me31B (Supplementary Movie S3). (d) Dynamic particles of *grk* (white arrowheads) are visualized docking and remaining on the edge of Me31B-rich zones. Other

small *grk* particles are seen in association with the Me31B throughout the time course (dashed cyan circles; Supplementary Movie S4). (e) *bcd*\**RFP*- and Me31B::GFP-expressing oocytes show *bcd* particles (white arrowheads) moving independently of Me31B (Supplementary Movie S5). (f) Average particle velocities for dynamic Me31B ( $n=30$ ), *grk* ( $n=37$ ) and *bcd* ( $n=31$ ) particles in micrometres per second  $\pm$  s.e.m.  $P$  values from Student's  $t$ -tests (two tails),  $P < 0.001$ . (g) FRAP of Me31B::GFP at the dorsoanterior corner shows recovery to approximately 50% of total fluorescence with a half-time of 4 min ( $n=5$ ). NC, nurse cell; N, nucleus. Scale bars, 10  $\mu\text{m}$  (a); 2  $\mu\text{m}$  (b–e); 20  $\mu\text{m}$  (g).

Although ISH–IEM provides excellent ultrastructural preservation and resolution, it represents only a two-dimensional view and has limited sensitivity of detection of RNA, because gold conjugates penetrate only the first 5 nm of the ultrathin 60 nm frozen section<sup>12</sup>. We, therefore, used the complementary method of three-dimensional structured illumination microscopy (3D-SIM), which provides double the conventional resolution of light microscopy in each dimension<sup>14</sup>. To co-visualize P bodies and mRNA, we detected P bodies with a GFP fusion to Me31B (Me31B::GFP; ref. 13) at the same time as tagging *grk* mRNA with 12 copies of the MS2 binding loop or *bcd* mRNA with 6 copies of MS2, both encoding functional genes<sup>2,15,16</sup>. The tagged mRNA was decorated with MS2-coat protein (MCP) fused to fluorescent proteins<sup>2,15–17</sup>, subsequently referred to as *grk*\**GFP*, *RFP* or *mCherry*). We found that *grk*\**mCherry* is excluded from the core of

the P bodies and interdigitates with Me31B::GFP, with a slight overlap at the interface, which we interpret as consistent with the ISH–IEM results (Fig. 1f). In contrast, *bcd*\**RFP* overlaps significantly with the P body core in both techniques (Fig. 1g).

We next investigated whether the differences we observe in the distribution of *grk* and *bcd* mRNAs relative to P bodies can be explained by their distinct transport and anchoring dynamics. We performed rapid single- and multi-colour wide-field fluorescence microscopy in living stage-8/9 oocytes (Fig. 2a–e and Supplementary Movies S1–S6). We observed three distinct populations of mRNA particles: active transport particles moving along linear paths characteristic of transport by molecular motors; paused transport particles showing a complex constrained motion; and docked *grk* statically associated with P bodies (Supplementary Fig. S3a,b). Active transport particles of *grk* mRNA

and *bcd* mRNA do not co-localize with Me31B, but rather move in the space between P bodies with an average velocity of  $0.5 \mu\text{m s}^{-1}$  (Fig. 2c,e,f and Supplementary Movies S4 and S6). Forty-one per cent of *grk* particles dock at the edge of P bodies (Fig. 2d and Supplementary Movie S5). In contrast, out of 155 *bcd* transport particles, none showed *grk*-like docking at the edge of the P bodies in stage-8/9 oocytes. A quantitative analysis of particle motility, by mean squared displacement (MSD) confirmed the difference between motile and docked particles (Supplementary Information and Methods). We suggest that *bcd* mRNA rapidly integrates into the P body core on contact with the P bodies, whereas *grk* mRNA particles remain docked on their outside.

Our co-visualization of mRNA and Me31B showed that mRNA particles move independently of Me31B. To determine whether Me31B is also dynamic and to establish how its distribution in P bodies is maintained, we first visualized Me31B::GFP at high time resolution. We observed Me31B::GFP particles moving with an average velocity of approximately  $0.25 \mu\text{m s}^{-1}$  (Fig. 2b,f and Supplementary Movies S2 and S3), significantly slower than RNA particles (Fig. 2f). This suggests that Me31B is in continual flux as small dynamic particles that leave or join larger Me31B-rich P bodies. We then examined the degree of exchange of Me31B in and out of P bodies using fluorescence recovery after photobleaching (FRAP) experiments. We found that Me31B::GFP recovers to approximately 50% of total fluorescence with a half-time of approximately 4 min after photobleaching (Fig. 2g). In contrast, control experiments using freely diffusing GFP fused to a nuclear localization signal (nlsGFP) recovered over 90% of total fluorescence in less than 5 s ( $n = 5$ , data not shown). We conclude that Me31B::GFP is not freely diffusible, but instead is maintained by relatively slow exchange of dynamic particles that move independently of *grk* and *bcd* mRNA.

To begin to understand how this organization could influence translation, we characterized the distribution of key translation components in the oocyte at mid-oogenesis (Fig. 3a–g and Supplementary Fig. S3c–k). Our results show that many factors involved in mRNA localization and translational regulation including Exuperantia (Exu), Trailer hitch (Tral) and Growl (also known as Lost) do not co-localize with *grk* mRNA but exhibit the same distribution as Me31B (Fig. 1f and Supplementary Fig. S3c–e). Similarly, Cup and Eukaryotic initiation factor 4E (eIF4E) co-localize with P bodies (Supplementary Fig. S3g–k). Furthermore, using IEM, we show that Me31B, Heterogeneous nuclear ribonucleoprotein at 27C (Hrb27C/Hrp48/p50) and the mRNA degradation enzyme Decapping protein 2 (Dcp2), a hallmark of P bodies in yeast and mammalian cells<sup>9</sup>, are significantly enriched in the P body core when compared with the surrounding cytoplasm, suggesting that the P body core is translationally silent (Fig. 3a–c, e and Supplementary Fig. S3f).

In line with the role of P bodies in translational inhibition, previous work showed that P bodies lack ribosomes, as judged by morphological analysis and by a GFP-tagged ribosomal component<sup>8,18</sup>. We confirmed this by labelling endogenous ribosomes by IEM using an antibody against a specific ribosomal protein (Fig. 3d,e and Supplementary Figs S4 and S2d and Methods). We found that 91% of ribosomes are not associated with P bodies. Interestingly, the 9% of ribosomes associated with the P bodies are almost exclusively enriched at the P body edge (Fig. 3e), and some of them are on endoplasmic reticulum (ER) strands closely apposed to P bodies (Fig. 3d). We conclude that the core of

oocyte P bodies cannot support translation, whereas the edge of P bodies could support translation, for instance, of *grk* mRNA.

To investigate this further, we examined the distribution of the translational activator Orb. Although Orb has not been shown to bind directly to *grk* mRNA, it is known to be required for *grk* mRNA localization and translation<sup>19</sup>. Our results show that Orb is enriched at the P body edge (Fig. 3e,f and Supplementary Fig. S2b'), suggesting that the edge of P bodies could be an Orb-mediated site of translational activation. We also determined the distribution of Sqd in P bodies, as it is required to maintain *grk* mRNA localization and we previously showed that it is present in P bodies and within *grk* RNP transport particles<sup>7</sup>. We used an anti-GFP antibody to detect Sqd::GFP and showed that Sqd is enriched 3.5 times at the P body edge when compared with its core (Fig. 3e,g). We conclude that in the oocyte, there is a distinct edge region of the P body that is competent for translation whereas the core is a site of translational repression. This is the first evidence suggesting a relationship between the P body stratified organization and the translational fates of distinct mRNAs.

To investigate directly whether the edge of P bodies is also the site of *grk* translation, we co-visualized *grk* mRNA and protein at the ultrastructural level. Our results show that, at the steady state, the intracellular pool of endogenous Grk protein is found in the early secretory pathway, within the ER and transitional ER (tER)–Golgi units. This distribution is in line with the fact that the Grk protein is first synthesized as a transmembrane protein, processed and secreted into the intracellular space between the oocyte and dorsoanterior follicle cells (Fig. 4a)<sup>12</sup>. Although Grk protein is largely found at a different location from its mRNA, we found a small amount of Grk protein is also present on rough ER (RER) at the edge of P bodies (Figs 4a,b and 3d) where *grk* mRNA is docked (Fig. 1b–d). We also observed *grk* mRNA transport particles lacking the Grk protein (see arrowhead in Fig. 4b) that are present at the dorsoanterior corner but are not docked to P bodies. Given that *grk* mRNA is repressed during transport<sup>5,20</sup>, we favour the interpretation that translational activation of *grk* mRNA occurs when transport particles dock at the edge of P bodies from where Grk protein enters the secretory pathway.

At steady state, most of the Grk protein is located in the secretory pathway<sup>12</sup>. Therefore, it is difficult to determine where *grk* mRNA is first translated. To overcome this, we injected a mixture of AlexaFluor-labelled RNA and unlabelled RNA encoding a full-length Grk protein into *grk*-mRNA-null oocytes<sup>5</sup> (Fig. 4c,d). Despite potentially not being subject to the normal translational repression while being transported, our results show that a pulse of Grk protein translation is co-localized with *grk* RNA, and both were interdigitated with Me31B (Fig. 4c, arrowheads). We interpret these results as showing that *grk* mRNA is translated at the P body edge.

Precise regulation of the dosage level of the Grk protein in the oocyte is essential for correct dorsoventral patterning<sup>20</sup>. To examine whether an excess of *grk* mRNA is translationally repressed, we injected varying amounts of *grk* RNA and characterized its distribution after localization. Injection is a well-established assay for monitoring RNA localization<sup>3,21</sup>. Despite being additional to endogenous *grk* mRNA, injected *grk* RNA assembles into transport particles that become localized at the dorsoanterior corner<sup>22</sup>. We show that moderate concentrations of injected *grk* RNA ( $\sim 120 \text{ ng } \mu\text{l}^{-1}$ ) localize and interdigitate with Me31B, at the edge of the P bodies (Supplementary Fig. S5a,b). In contrast, injecting

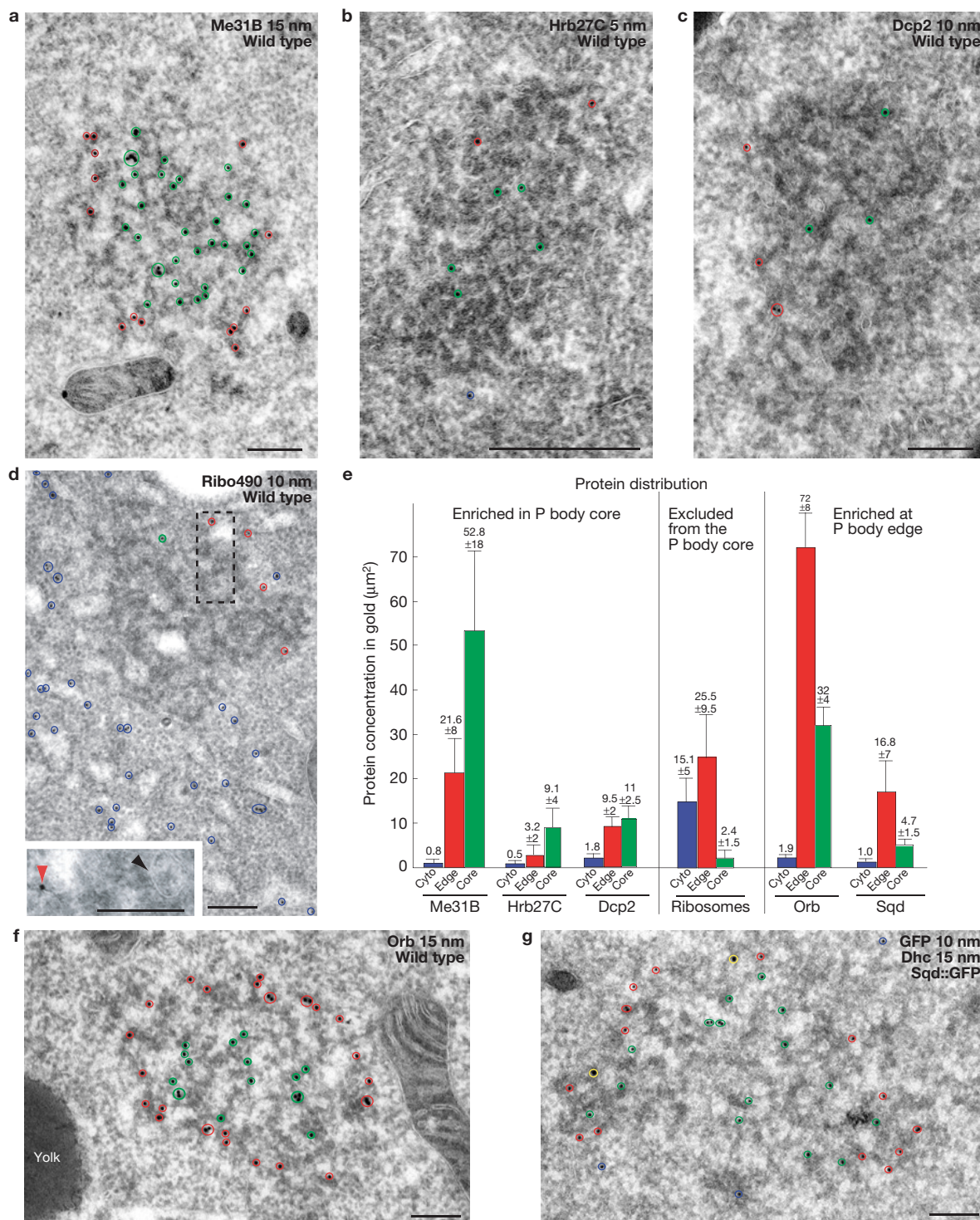


**Figure 3** Oocyte P bodies exhibit zones differentially enriched in RNA-associated proteins. (**a–d,f,g**) IEM localization of RNA-associated proteins in stage-9 oocytes at the dorsoanterior corner. Protein in the core of the electron-dense P bodies is indicated by green circles, at the edge of P bodies by red circles and in the cytoplasm by blue circles. (**a**) Wild-type egg chamber, anti-Me31B (15 nm) enriched inside P bodies. (**b**) Hrb27C (5 nm) predominantly inside P bodies. (**c**) Dcp2 (10 nm) inside and at the edge of P bodies. (**d**) Wild-type egg chamber, anti-Ribo 490 (10 nm) shows ribosomes predominantly in the cytoplasm, some at the edge but mostly excluded from inside P bodies. The pool of cytoplasmic ribosomes corresponds to polysomes

and those present on the ER membrane (RER), some of which is present near the edge of a P body (black dashed rectangle, inset: red arrowhead). Smooth ER is detected inside the P body (inset: black arrowhead). (**e**) Graph showing protein concentration in gold  $\mu\text{m}^{-2}$  in the cytoplasm, edge of P bodies and inside P bodies; proteins are organized into three distinct categories. Error bars are  $\pm$ s.d. (between  $n = 10$ – $15$  scans in each case). (**f**) Wild-type egg chamber, anti-Orb (15 nm) enriched at the edge of P bodies. (**g**) Sqd-GFP in Sqd::GFP-expressing egg chamber using anti-GFP (10 nm) and anti-Dhc (15 nm, yellow circles). Sqd is enriched inside when compared with at the edge of P bodies. Scale bars, 200 nm (**a–d,f,g**).

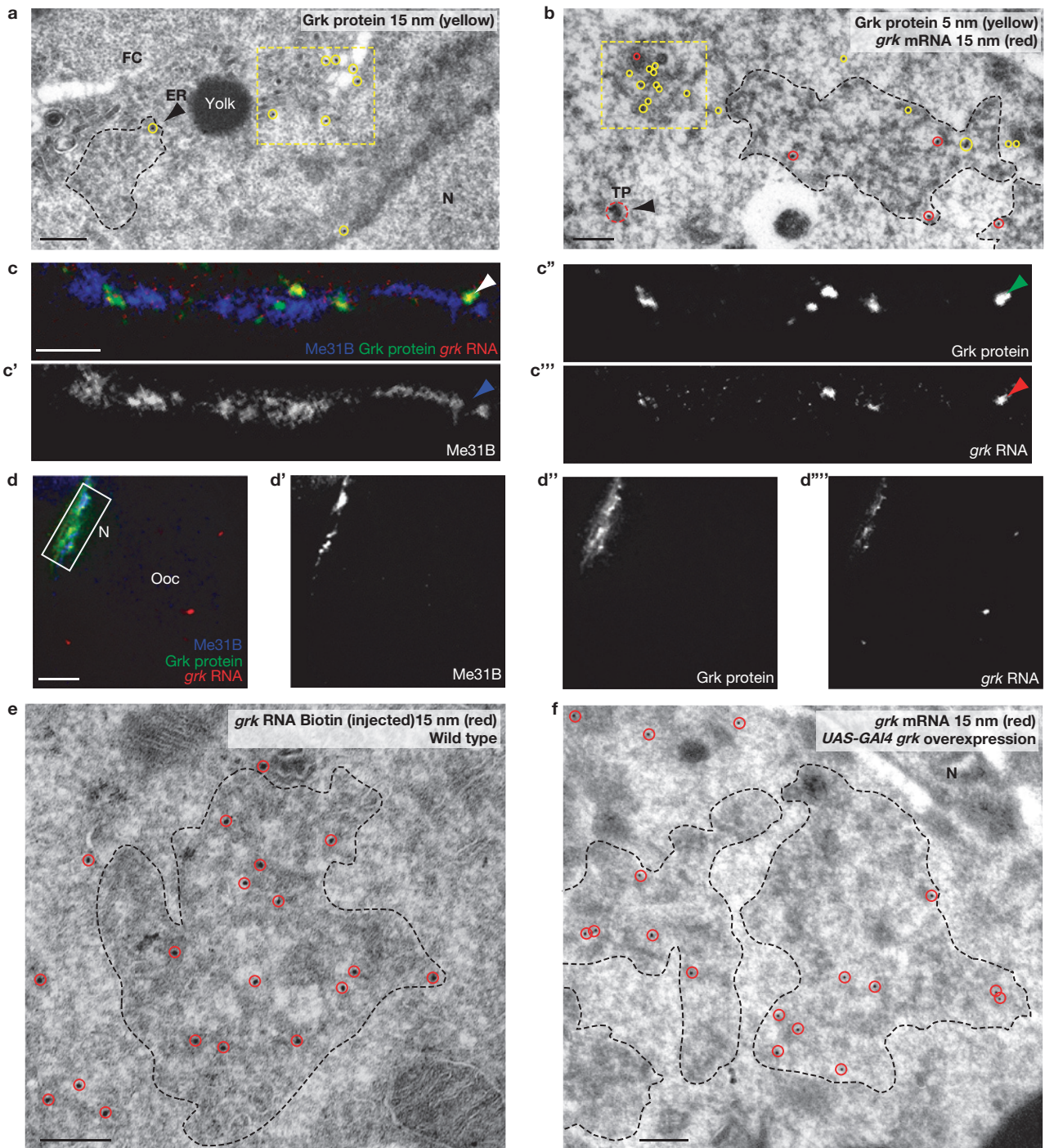


**Figure 4** RNA translation fate is regulated through association with P bodies (marked with a dashed black line). (a) IEM using anti-Grk (15 nm, yellow circles) on a wild-type stage-9 egg chamber shows Grk protein highly enriched in the tER–Golgi unit (yellow dashed rectangle) and detected on the ER (black arrowhead) at the edge of a P body. (b) ISH–IEM detection of *grk* mRNA and Grk protein on a wild-type stage-9 egg chamber shows *grk* mRNA (15 nm, red circles) mostly present at the edge of the P body and Grk protein (5 nm, yellow circles) on a tER–Golgi unit (yellow dashed rectangle) but also present at the edge of the P body. Note the *grk* mRNA transport particle (dashed red circle) does not contain any detectable Grk protein (black arrowhead). (c) Injection of *in vitro*-synthesized *grk* RNA (mixed solution of approximately one part Alexa dye labelled and four parts unlabelled) into a *grk*-null egg chamber expressing Me31B::GFP. Images shown are

a 4  $\mu$ m projection. Localization and translation was allowed for 40 min before the egg chamber was fixed and labelled with anti-Grk. Grk protein (green; c,c'') and *grk* RNA (red; c,c'') co-localize, but do not co-localize with Me31B (blue; c,c'). Instead, *grk* RNA and protein interdigitates with Me31B (arrowheads). (d) Low-magnification images of c. Injected *grk* RNA is localized to the dorsoanterior corner where it is translated. (e) IEM on a wild-type stage-8/9 egg chamber injected with a high concentration of *grk* RNA Biotin (500  $\text{ng } \mu\text{l}^{-1}$ ). Injected RNA (15 nm, red circles) is detected at the core of and at the edge of the P body. (f) IEM on a stage-8/9 egg chamber overexpressing *grk* mRNA using the UAS–Gal4 system. *grk* mRNA (15 nm, red circles) is enriched at the core of and at the edge of the P body. FC, follicle cell; TP, transport particle; ER, endoplasmic reticulum; N, nucleus; Ooc, oocyte. Scale bars, 200 nm (a,b,e,f); 3  $\mu$ m (c); 10  $\mu$ m (d).

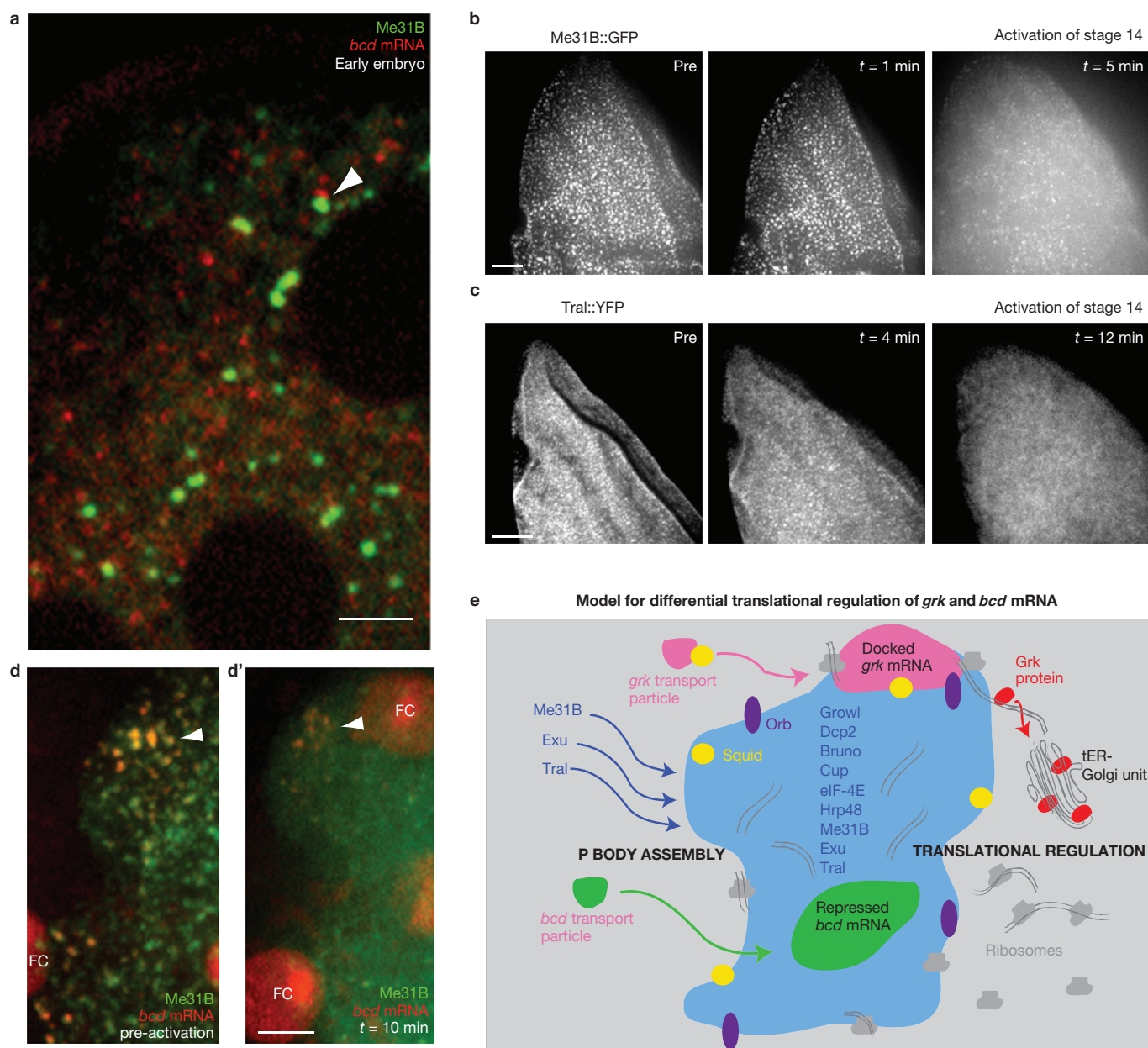


**Figure 5** RNA association with P bodies in the early embryo. **(a)** Anterior region of a live early embryo expressing *bcd\* RFP* and Me31B::GFP. *bcd* mRNA is mainly detected outside Me31B labelling, sometimes associating with the edge (arrowhead). **(b,c)** Time points from a stage-14 egg chamber expressing Me31B::GFP **(b)** or Tral::YFP **(c)**, before and following activation. Activation buffer added at  $t = 0$  min. Immediately after activation, Me31B (or Tral)-labelled P bodies disperse. **(d)** Stage-14 egg chamber expressing *bcd\* RFP* and Me31B::GFP, before treatment with activation buffer **(d)** and 10 min after activation buffer is applied **(d')**. Pre-activation, *bcd* mRNA and Me31B co-localize at the anterior (arrowhead). Immediately after activation, Me31B disperses and *bcd* no longer co-localizes with Me31B (arrowhead). **(e)** Model of how P bodies regulate differential

translation of *bcd* and *grk* mRNA at the dorsoanterior corner in a stage-8/9 oocyte. *grk* mRNA transport particles move independently of Me31B. *grk* associates at the edge of the P body where enrichment of Sqd is involved in anchoring, Orb activates translation and ribosomes support translation. *grk* is translated on RER at the edge of P bodies and Grk protein is trafficked through the secretory pathway (tER–Golgi unit) before being secreted. *bcd* mRNA transport particles move independently of Me31B and associate with the core of the P body where translation is not supported. Dynamic Me31B, Exu and Tral particles assemble and maintain the P bodies. Excess *grk* RNA is targeted into the core of P bodies where it is translationally repressed and probably degraded. FC, follicle cell. Scale bars, 5  $\mu$ m **(a,d)**; 20  $\mu$ m **(b,c)**.

fourfold more *grk* RNA leads a proportion of RNA localizing to the core of P bodies (Fig. 4e and Supplementary Fig. S5c,d). We conclude that an excess of injected *grk* RNA is directed to the P body core.

To investigate whether an excess of endogenous *grk* mRNA behaves like injected RNA, we used the UAS–Gal4 system to drive *grk* overexpression. We confirmed that overexpression occurred with

anti-Grk antibodies and *grk* FISH (Supplementary Fig. S5e,f), and found dorsoventral patterning defects in eggs to varying degrees<sup>23</sup>. We used ISH–IEM to determine where overexpressed *grk* mRNA is localized and found a clear increase in the relative proportion of *grk* mRNA found in the core of P bodies when compared with the wild type (Fig. 4f and Supplementary Fig. S5g,h). Together, these results support

a model where excess *grk* mRNA is directed into the core of the P body, which lacks ribosomes and maintains translational repression.

To further examine the relationship between P body sub-localization and differential translation, we analysed translationally repressed *bcd* mRNA in oocytes and translationally active *bcd* mRNA in embryos<sup>6</sup>. At stage 9 of oogenesis, a population of *bcd* is enriched in the P body core (Fig. 1), whereas the remainder is in highly dynamic particles that are known to also be translationally repressed by a mechanism that is not well understood. At stage 14 of oogenesis, when *bcd* mRNA is known to be anchored and repressed<sup>6,24</sup>, all of it co-localizes with Me31B (Supplementary Fig. S5i,j). In contrast, in early embryos, at a time when it is translated, *bcd* mRNA is outside P bodies (Fig. 5a). It is not known when and how *bcd* translation is activated in embryos, but we propose that this may be related to egg activation, a major transition point between oocytes and embryos.

We previously showed that *bcd* mRNA is released from its anterior cytoskeletal anchor by egg activation<sup>24</sup>. To examine whether egg activation is also the trigger for *bcd* mRNA redistributing outside the P bodies, we co-visualized labelled P bodies and *grk*<sup>\*</sup>MS2, before and after activating eggs *in vitro*. We found that on egg activation, Me31B (Fig. 5b) and Tral (Fig. 5c) become dispersed, resulting in a loss of co-localization between *bcd* mRNA and Me31B (Fig. 5d,d'). Although our data do not address directly whether the translational activation of *bcd* mRNA is caused by P body disassembly, we previously showed that in *sarah* mutant embryos, where activation does not occur, *bcd* mRNA is not released from the anterior or translated<sup>24,25</sup>. Therefore, we propose that translational activation of *bcd* mRNA results from the disassembly of P bodies on egg activation.

Our results demonstrate the stratification of P bodies and suggest how localized transcripts could be differentially translated by distinct associations with P body zones. We propose a model for the spatio-temporal regulation of the translation of developmentally important mRNAs in the oocyte (Fig. 5e). Translationally repressed RNP transport particles associate with the edge of P bodies where anchoring and translation activation factors, such as Sqd and Orb, are enriched. We previously showed that disrupting Sqd function causes a defect in anchoring of transport particles at the dorsoanterior P bodies<sup>7</sup>. Instead of docking at the dorsoanterior corner, *grk* transport particles are in continuous flux along the anterior and *grk* is inappropriately translated<sup>7</sup>. We therefore favour a model in which *sqd* is required for translational repression of *grk* mRNA during its transport, and for anchoring the transcript at the P body edge. In this model, Orb is also present at the edge P bodies and is required for translational activation of *grk* mRNA. RNA, such as *grk*, that are excluded from the core of the P body are translationally activated at the edge. In contrast, *bcd* and probably other transcripts that enter the ribosome-depleted core of P bodies remain translationally repressed. Furthermore, the finding that excess *grk* RNA leads to an increase in the proportion of *grk* in the P body core leads us to speculate that this is a mechanism for regulating Grk protein levels.

P bodies are one of several related electron-dense and RNP-rich cellular structures<sup>26</sup> that include stress granules<sup>27</sup>, the *Xenopus* mitochondrial cloud<sup>28</sup>, the zebrafish Balbiani body<sup>29</sup> and nematode P granules<sup>30</sup>. The dynamic nature of the protein and mRNA components of these structures has not often been studied in detail, except in *Caenorhabditis elegans* where P granules have been shown to behave in a fluid-like manner<sup>31</sup>. Our observation of highly dynamic

independent movements of a P body protein and mRNA provides a general molecular basis for the fluid-like behaviour of P granules and related granules. There has been considerable debate about whether P body formation is essential for mRNA decay and translational repression or a consequence of these events<sup>32–35</sup>. The consensus has been that P body formation is essential for mRNA decay and translational repression<sup>5,32–34</sup> and our work highlights another function for P bodies in translational regulation of key transcripts through partitioning between the core and edge of the bodies. □

## METHODS

Methods and any associated references are available in the online version of the paper.

*Note: Supplementary Information is available in the online version of the paper*

## ACKNOWLEDGEMENTS

We are grateful to: E. R. Gavis (Princeton University, USA), D. Ish-Horowicz (CRUK, UK), T. Schüpbach (Princeton University, USA), A. Jaramillo (Princeton University, USA), J. van Minnen (University of Calgary, Canada), L. Cooley (Yale University, USA), R. Singer (Albert Einstein College of Medicine, USA) and A. Nakamura (RIKEN, Japan) for fly stocks, antibodies and reagents; all members of the Cell Microscopy Center in Utrecht, Netherlands for assistance with electron microscopy; J. W. Sedat (UCSF, USA) and D. Agard (UCSF, USA) for advise on super-resolution imaging; E. R. Gavis for experimental advice; A. Ephrussi (EMBL, Germany) for discussions of the data. This work was supported by: Marie Curie International Incoming Fellowship (ROXA0) to T.T.W.; Wellcome Trust Senior Research Fellowship (081858) to I.D. and supporting R.M.P. and T.T.W.; Cancer Research UK funding to R.H.; studentship from Wellcome Trust to J.M.H.; Darwin Trust to J.S.

## AUTHOR CONTRIBUTIONS

T.T.W., R.M.P., C.R. and I.D. provided the intellectual basis of the work and designed the experiments. T.T.W., R.M.P., B.H., D.X. and T.V. performed experiments resulting in figures. J.S., R.H. and J.M.H. performed experiments that contributed intellectually but did not result in figures. R.H. generated reagents. I.M.D. and R.M.P. provided technical expertise for equipment, advanced microscopy and data analysis. T.T.W., R.M.P., C.R. and I.D. wrote and edited the manuscript.

## COMPETING FINANCIAL INTERESTS

The authors declare no competing financial interests.

Published online at [www.nature.com/doi/10.1038/ncb2627](http://www.nature.com/doi/10.1038/ncb2627)

Reprints and permissions information is available online at [www.nature.com/reprints](http://www.nature.com/reprints)

1. St Johnston, D. Moving messages: the intracellular localization of mRNAs. *Nat. Rev. Mol. Cell Biol.* **6**, 363–375 (2005).
2. Weil, T. T., Forrest, K. M. & Gavis, E. R. Localization of bicoid mRNA in late oocytes is maintained by continual active transport. *Dev. Cell* **11**, 251–262 (2006).
3. Cha, B. J., Koppetsch, B. S. & Theurkauf, W. E. *In vivo* analysis of *Drosophila* bicoid mRNA localization reveals a novel microtubule-dependent axis specification pathway. *Cell* **106**, 35–46 (2001).
4. Clark, A., Meignin, C. & Davis, I. A Dynein-dependent shortcut rapidly delivers axis determination transcripts into the *Drosophila* oocyte. *Development* **134**, 1955–1965 (2007).
5. Neuman-Silberberg, F. S. & Schüpbach, T. The *Drosophila* dorsoventral patterning gene *gurken* produces a dorsally localized RNA and encodes a TGF $\alpha$ -like protein. *Cell* **75**, 165–174 (1993).
6. St Johnston, D., Driever, W., Berleth, T., Riechstein, S. & Nüsslein-Volhard, C. Multiple steps in the localization of *bicoid* RNA to the anterior pole of the *Drosophila* oocyte. *Development* **107** (Suppl.), 13–19 (1989).
7. Delanoue, R., Herpers, B., Soetaert, J., Davis, I. & Rabouille, C. *Drosophila* Squid/hnRNP helps Dynein switch from a gurken mRNA transport motor to an ultrastructural static anchor in sponge bodies. *Dev. Cell* **13**, 523–538 (2007).
8. Wilsch-Brauninger, M., Schwarz, H. & Nüsslein-Volhard, C. A sponge-like structure involved in the association and transport of maternal products during *Drosophila* oogenesis. *J. Cell Biol.* **139**, 817–829 (1997).
9. Snee, M. J. & Macdonald, P. M. Dynamic organization and plasticity of sponge bodies. *Dev. Dyn.* **238**, 918–930 (2009).
10. Beckham, C. *et al.* The DEAD-box RNA helicase Ded1p affects and accumulates in *Saccharomyces cerevisiae* P-bodies. *Mol. Biol. Cell* **19**, 984–993 (2008).

11. Minshall, N., Kress, M., Weil, D. & Standart, N. Role of p54 RNA helicase activity and its C-terminal domain in translational repression, P-body localization and assembly. *Mol. Biol. Cell* **20**, 2464–2472 (2009).
12. Herpers, B. & Rabouille, C. mRNA localization and ER-based protein sorting mechanisms dictate the use of transitional endoplasmic reticulum–Golgi units involved in gurken transport in *Drosophila* oocytes. *Mol. Biol. Cell* **15**, 5306–5317 (2004).
13. Nakamura, A., Amikura, R., Hanyu, K. & Kobayashi, S. Me31B silences translation of oocyte-localizing RNAs through the formation of cytoplasmic RNP complex during *Drosophila* oogenesis. *Development* **128**, 3233–3242 (2001).
14. Dobbie, I. *et al.* in *Live Cell Imaging: A Laboratory Manual* Second edn (eds Goldman, Robert D., Swedlow, Jason R. & Spector, David L.) 203–214 (Cold Spring Harbor Laboratory Press, 2010).
15. Jaramillo, A. M., Weil, T. T., Goodhouse, J., Gavis, E. R. & Schüpbach, T. The dynamics of fluorescently labeled endogenous gurken mRNA in *Drosophila*. *J. Cell Sci.* **121**, 887–894 (2008).
16. Forrest, K. M. & Gavis, E. R. Live imaging of endogenous RNA reveals a diffusion and entrapment mechanism for nanos mRNA localization in *Drosophila*. *Curr. Biol.* **13**, 1159–1168 (2003).
17. Bertrand, E. *et al.* Localization of ASH1 mRNA particles in living yeast. *Mol. Cell* **2**, 437–445 (1998).
18. Teixeira, D., Sheth, U., Valencia-Sanchez, M. A., Brengues, M. & Parker, R. Processing bodies require RNA for assembly and contain nontranslating mRNAs. *RNA* **11**, 371–382 (2005).
19. Chang, J. S., Tan, L., Wolf, M. R. & Schedl, P. Functioning of the *Drosophila* orb gene in gurken mRNA localization and translation. *Development* **128**, 3169–3177 (2001).
20. Neuman-Silberberg, F. S. & Schüpbach, T. Dorsoventral axis formation in *Drosophila* depends on the correct dosage of the gene gurken. *Development* **120**, 2457–2463 (1994).
21. Wilkie, G. S. & Davis, I. *Drosophila* wingless and pair-rule transcripts localize apically by dynein-mediated transport of RNA particles. *Cell* **105**, 209–219 (2001).
22. MacDougall, N., Clark, A., MacDougall, E. & Davis, I. *Drosophila* gurken (TG $\alpha$ ) mRNA localizes as particles that move within the oocyte in two dynein-dependent steps. *Dev. Cell* **4**, 307–319 (2003).
23. Bokel, C., Dass, S., Wilsch-Brauninger, M. & Roth, S. *Drosophila* Cornichon acts as cargo receptor for ER export of the TG $\alpha$ -like growth factor Gurken. *Development* **133**, 459–470 (2006).
24. Weil, T. T., Parton, R., Davis, I. & Gavis, E. R. Changes in bicoid mRNA anchoring highlight conserved mechanisms during the oocyte-to-embryo transition. *Curr. Biol.* **18**, 1055–1061 (2008).
25. Horner, V. L. *et al.* The *Drosophila* calcipressin sarah is required for several aspects of egg activation. *Curr. Biol.* **16**, 1441–1446 (2006).
26. Moser, J. J. & Fritzler, M. J. Cytoplasmic ribonucleoprotein (RNP) bodies and their relationship to GW/P bodies. *Int. J. Biochem. Cell Biol.* **42**, 828–843 (2010).
27. Buchan, J. R. & Parker, R. Eukaryotic stress granules: the ins and outs of translation. *Mol. Cell* **36**, 932–941 (2009).
28. King, M. L., Messitt, T. J. & Mowry, K. L. Putting RNAs in the right place at the right time: RNA localization in the frog oocyte. *Biol. Cell* **97**, 19–33 (2005).
29. Kloc, M., Bilinski, S. & Etkin, L. D. The Balbiani body and germ cell determinants: 150 years later. *Curr. Top Dev. Biol.* **59**, 1–36 (2004).
30. Updike, D. & Strome, S. P granule assembly and function in *Caenorhabditis elegans* germ cells. *J. Androl.* **31**, 53–60 (2010).
31. Brangwynne, C. P. *et al.* Germline P granules are liquid droplets that localize by controlled dissolution/condensation. *Science* **324**, 1729–1732 (2009).
32. Eulalio, A., Behm-Ansmant, I., Schweizer, D. & Izaurralde, E. P-body formation is a consequence, not the cause, of RNA-mediated gene silencing. *Mol. Cell Biol.* **27**, 3970–3981 (2007).
33. Parker, R. & Sheth, U. P bodies and the control of mRNA translation and degradation. *Mol. Cell* **25**, 635–646 (2007).
34. Balagopal, V. & Parker, R. Polysomes, P bodies and stress granules: states and fates of eukaryotic mRNAs. *Curr. Opin. Cell Biol.* **21**, 403–408 (2009).
35. Stoecklin, G., Mayo, T. & Anderson, P. ARE-mRNA degradation requires the 5'-3' decay pathway. *EMBO Rep.* **7**, 72–77 (2006).

## METHODS

**Fly strains.** Stocks were raised on standard cornmeal–agar medium at 21 or 25 °C. The wild type was Oregon R (OrR). P body markers: *Me31B::GFP* (ref. 36; CG4916); *Growl::GFP* (ref. 36; CG14648), *eIF-4E::GFP* (ref. 36; CG4035), *Exu::GFP* (ref. 37; CG8994), *Tral::YFP* (D. St Johnston; CG10686), *SquidGFP* (ref. 38; CG16901). Overexpression lines: maternal tubulin: Gal4–VP16 driver; UASpGrkmyc (ref. 23). *MS2–MCP(FP)* lines: *hsp83–NLS–MCP–GFP* (ref. 16); *Pnos–NLS–MCP–mCherry*; *grk – (MS2)<sup>12(15)</sup>*; *hsp83–MCP–RFP<sup>2</sup>*, *bcd–(MS2)<sup>6(2)</sup>*. Mutant lines: *grk<sup>266</sup>* and *grk<sup>2e12(5)</sup>*.

**Electron microscopy sample preparation and analysis.** *grk* and *bcd* mRNAs were detected using methods previously described<sup>7,39</sup>. Images were captured on a Jeol EX1200 electron microscope. Protein detection was performed by IEM as described previously<sup>40</sup>. Analysis of electron micrographs was done first by manually defining the P body outline<sup>9</sup> on the basis of electron density. To objectively characterize the organization of P bodies, we applied concentric regions of interest to the P body outline at 20 nm increments (Supplementary Fig. S2a–a’). For consistency we measured to a total distance inside the P body of 160 nm, as dictated by the size of the smallest P bodies analysed. The number of gold particles in each concentric area was counted as previously described<sup>41</sup>. To facilitate comparison, the area was calculated for each region of interest and the corresponding density of gold determined.

On the basis of the Me31B and Orb density plots, two zones were defined and used for subsequent comparisons: edge, the outermost electron-dense material containing most of the Orb and minimal Me31B as shown in density plots (Supplementary Fig. S2b–b’), corresponding to approximately 70 nm inside the P body outline; core, defined as containing most of the Me31B. From our analysis, we estimate that the edge zone represents 25% of the total volume for a typical 1- $\mu$ m-diameter P body. Randomized particles are without scale bars because density data were pooled. For the distribution of ribosomes  $n = 500$  gold particles counted from 14 scans. *P* values are from Student’s *t*-tests (two tails).

**Antibodies.** Antibodies used: Grk, mouse monoclonal, clone no. 1D12 (Developmental Studies Hybridoma Bank, 1:30); Me31B, mouse monoclonal (gift from A. Nakamura<sup>13</sup>, 1:1,000); Cup, mouse monoclonal (gift from A. Nakamura, 1:1,000); Bruno, rat polyclonal (gift from A. Ephrussi<sup>42</sup>, 1:300); Hrb27C, rabbit polyclonal (gift from D. Rio<sup>43</sup>, 1:500); Orb, mouse monoclonal, clone no. 4H8 (Developmental Studies Hybridoma Bank, 1:20); DCP2, rabbit polyclonal (gift from E. Izauralde<sup>44</sup>, 1:100); GFP, rabbit polyclonal, cat. no. A6455 (Molecular Probes, 1:300); RFP–Booster, cat. no. rba594 (Chromotek, 1:200); ribosomes, human polyclonal against  $\alpha$  Ribo-490 (gift from J. van Minnen, 1:300). Ribosomal proteins are highly conserved and this antibody has been used in other species<sup>45</sup>. Furthermore, the density of ribosomes we have detected on sections of *Drosophila* oocytes (Supplementary Fig. S4) and several other fly tissues (unpublished) is comparable to that detected on mammalian tissues and cells. Finally, the labelling is present in the cytoplasm and on ER membrane, where ribosomes are expected to be found. Therefore, we are confident that this antibody detects ribosomes in the *Drosophila* oocyte.

*In situ* digoxigenin (DIG)-labelled probe was detected with sheep anti-DIG Fab fragments coupled to HRP (DIG–HRP), cat. no. 11207733910 (Roche, 1:1,000) in ISH–IEM (ref. 39); injected biotinylated RNA was detected with polyclonal rabbit anti-biotin, cat. no. 100-401-B21 (Rockland, 1:10,000) in IEM and with AlexaFluor-546-coupled avidin, cat. no. S11225 (Molecular Probes) for light fluorescence microscopy; rabbit polyclonal antibodies were detected with protein-A gold conjugates (Department of Cell Biology, Institute of Bio-membranes, Utrecht, The Netherlands) in IEM and mouse monoclonals were first detected with rabbit anti-mouse, cat. no. D031402-2 (Dako, 1:250) followed by protein-A gold conjugates. Bridging antibodies lead to clustering of gold particles.

**Fluorescence imaging.** Flies were prepared and ovaries dissected and mounted for imaging according to standard protocols<sup>7,46,47</sup>. Imaging was performed either on an OMX-V2 prototype microscope (fast-live and 3D-SIM) designed by J. Sedat and built by Applied Precision (GE Healthcare)<sup>14</sup> or a Perkin-Elmer Ultraview VOX spinning-disc confocal microscope (Olympus IX81 microscope,  $\times 60$  1.3 NA SI objective, Hamamatsu C9100-13 EMCCD camera). Where required, image sequences were deconvolved with the SoftWoRx Resolve 3D constrained iterative deconvolution algorithm (Applied Precision). Basic image processing was carried out using Fiji (V1.0, <http://fiji.sc/wiki/index.php/Fiji>). MSD analysis was performed according ref. 48. MSD curves were assessed in terms of relative deviation (RD = observed MSD/extrapolated MSD) as described previously<sup>49</sup>. Super-resolution structured illumination reconstruction was performed as published previously<sup>14</sup>. For structured illumination a RFP–Booster for labelling RFP-fusion protein was used (Chromotek). The RFP–Booster is conjugated to an ATTO594 dye and recognizes both mCherry

and mRFP. Note, although the 3D-SIM data represent a projection of several fluorescence optical sections totalling 675 nm, the ISH–IEM sections are 60 nm thick, of which only the 5 nm surface is estimated to be accessible by gold conjugates.

**Live-cell imaging.** Two copies of *grk–(MS2)* (ref. 12) or *bcd–(MS2)* (ref. 6) were used with one copy of *MS2–MCP(FP)* for optimal imaging without phenotypic effects. The amount of *grk* RNA versus *bcd* RNA varies significantly with the plane of focus. Generally, the focal plane was selected for best optical imaging. Quantification of RNA particle average velocities was done in softWoRx (Applied Precision). *P* values are from Student’s *t*-tests (two tails). Docking is defined as a dynamic *grk* RNA particle moving into association with an Me31B-labelled P body or fusing with a *grk* RNP that is already associated with Me31B; for analysis of docking, all moving *grk* particles in a 50  $\mu$ m  $\times$  50  $\mu$ m area over 50 frames ( $\sim 17$  s) were examined. Diffusion in dense cytoplasm was determined based upon previous analysis<sup>30</sup>. FRAP was performed on a PerkinElmer UltraVIEW spinning-disc confocal microscope, 20  $\mu$ m  $\times$  20  $\mu$ m area bleached with recovery analysis completed in Velocity (PerkinElmer). Activation was performed as previously described<sup>24</sup>. Embryos were collected at 0–2 h and imaged according to standard protocols<sup>46</sup>.

**MSD analysis.** MSD (ref. 49) analysis of particle dynamics was used to definitively characterize and distinguish the different classes of *grk* mRNA particles (see Supplementary Fig. S3).

**Injection of RNA.** RNA was transcribed *in vitro* according to standard protocols<sup>21</sup>. Flies were prepared and ovaries dissected and mounted for imaging as previously described<sup>46,47</sup> and injected with labelled *grk* RNA using Femtotip needles (Eppendorf). RNA was injected at a concentration of  $\sim 120$  and  $\sim 500$  ng  $\mu$ l<sup>-1</sup> as measured by a NanoDrop ND-1000 spectrophotometer. Injected egg chambers were either imaged live as described above or fixed and processed for *grk* mRNA *in situ* hybridization.

**Immunofluorescence and RNA FISH.** Ovaries were dissected into 4% paraformaldehyde (PFA) in PBS (from fresh 16% stock solution; Polysciences) and fixed for 15 min (ref. 16). Injected oocytes were similarly fixed by adding fixative directly on top of the egg chambers in halocarbon oil<sup>7</sup>. Post-fixation was performed with 4% PFA for 20 min, followed by several washes with PBT (PBS + 0.1% Tween). After fixation, ovaries were processed for FISH and immunolabelled as previously described<sup>7,21</sup> or prepared for electron microscopy according to standard methods<sup>7,12</sup>.

36. Buszczak, M. *et al.* The Carnegie protein trap library: a versatile tool for *Drosophila* developmental studies. *Genetics* **175**, 1505–1531 (2007).
37. Theurkauf, W. E. & Hazelrigg, T. I. *In vivo* analyses of cytoplasmic transport and cytoskeletal organization during *Drosophila* oogenesis: characterization of a multi-step anterior localization pathway. *Development* **125**, 3655–3666 (1998).
38. Norvell, A., Debec, A., Finch, D., Gibson, L. & Thoma, B. Squid is required for efficient posterior localization of oskar mRNA during *Drosophila* oogenesis. *Dev. Genes Evol.* **215**, 340–349 (2005).
39. Herpers, B., Xanthakis, D. & Rabouille, C. ISH–IEM: a sensitive method to detect endogenous mRNAs at the ultrastructural level. *Nat. Protoc.* **5**, 678–687 (2010).
40. Slot, J. W. & Geuze, H. J. Cryosectioning and immunolabeling. *Nat. Protoc.* **2**, 2480–2491 (2007).
41. Rabouille, C. Quantitative aspects of immunogold labeling in embedded and nonembedded sections. *Methods Mol Biol.* **117**, 125–144 (1999).
42. Filardo, P. & Ephrussi, A. Bruno regulates gurken during *Drosophila* oogenesis. *Mech. Dev.* **120**, 289–297 (2003).
43. Hammond, L. E., Rudner, D. Z., Kanaar, R. & Rio, D. C. Mutations in the *hrp48* gene, which encodes a *Drosophila* heterogeneous nuclear ribonucleoprotein particle protein, cause lethality and developmental defects and affect P-element third-intron splicing *in vivo*. *Mol. Cell Biol.* **17**, 7260–7267 (1997).
44. Rehwinkel, J., Behm-Ansmant, I., Gatfield, D. & Izauralde, E. A crucial role for GW182 and the DCP1:DCP2 decapping complex in miRNA-mediated gene silencing. *RNA* **11**, 1640–1647 (2005).
45. Court, F. A., Hendriks, W. T., MacGillavry, H. D., Alvarez, J. & van Minnen, J. Schwann cell to axon transfer of ribosomes: toward a novel understanding of the role of glia in the nervous system. *J. Neurosci.* **38**, 11024–11029 (2008).
46. Parton, R. M., Valles, A. M., Dobbie, I. M. & Davis, I. Live cell imaging in *Drosophila melanogaster*. *Cold Spring Harb. Protoc.* **2010**, 387–418 (2010).
47. Weil, T. T., Parton, R. M. & Davis, I. Preparing individual *Drosophila* egg chambers for live imaging. *J. Vis. Exp.* <http://dx.doi.org/10.3791/3679> (2012).
48. Gross, D. J. & Webb, W. W. *Spectroscopic Membrane Probe, Vol. II*. 19–48 (CRC Press Inc., 1988).
49. Saxton, M. J. & Jacobson, K. Single-particle tracking: applications to membrane dynamics. *Annu. Rev. Biophys. Biomol. Struct.* **26**, 373–399 (1997).
50. Tadokuma, H., Ishihama, Y., Shibuya, T., Tani, T. & Funatsu, T. Imaging of single mRNA molecules moving within a living cell nucleus. *Biochem. Biophys. Res. Commun.* **344**, 772–779 (2006).

DOI: 10.1038/ncb2627

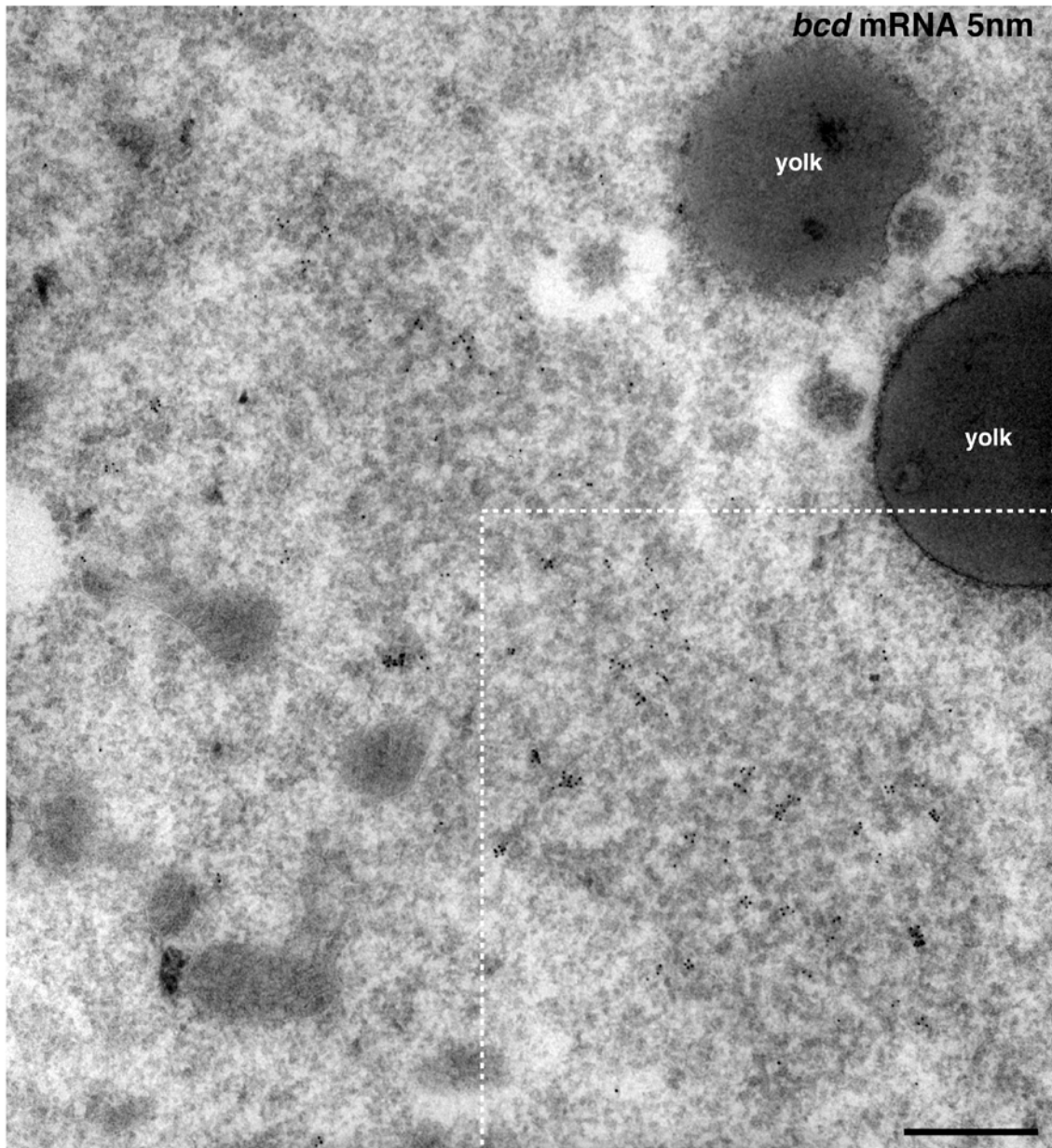


**Figure S1** *bcd* mRNA inside P bodies. A full sized scan of Fig. 1a, highlighting minimal gold in the cytoplasm. White dashed box indicates corresponding subregion in Fig. 1a. *bcd* mRNA detection at the dorsoanterior

corner by ISH-IEM on WT ultra-thin frozen sections of stage 9 oocytes. *bcd* mRNA (5nm gold) is enriched at the core and at the edge of electron dense P bodies which appear darker in color. Scale bar, 500nm.

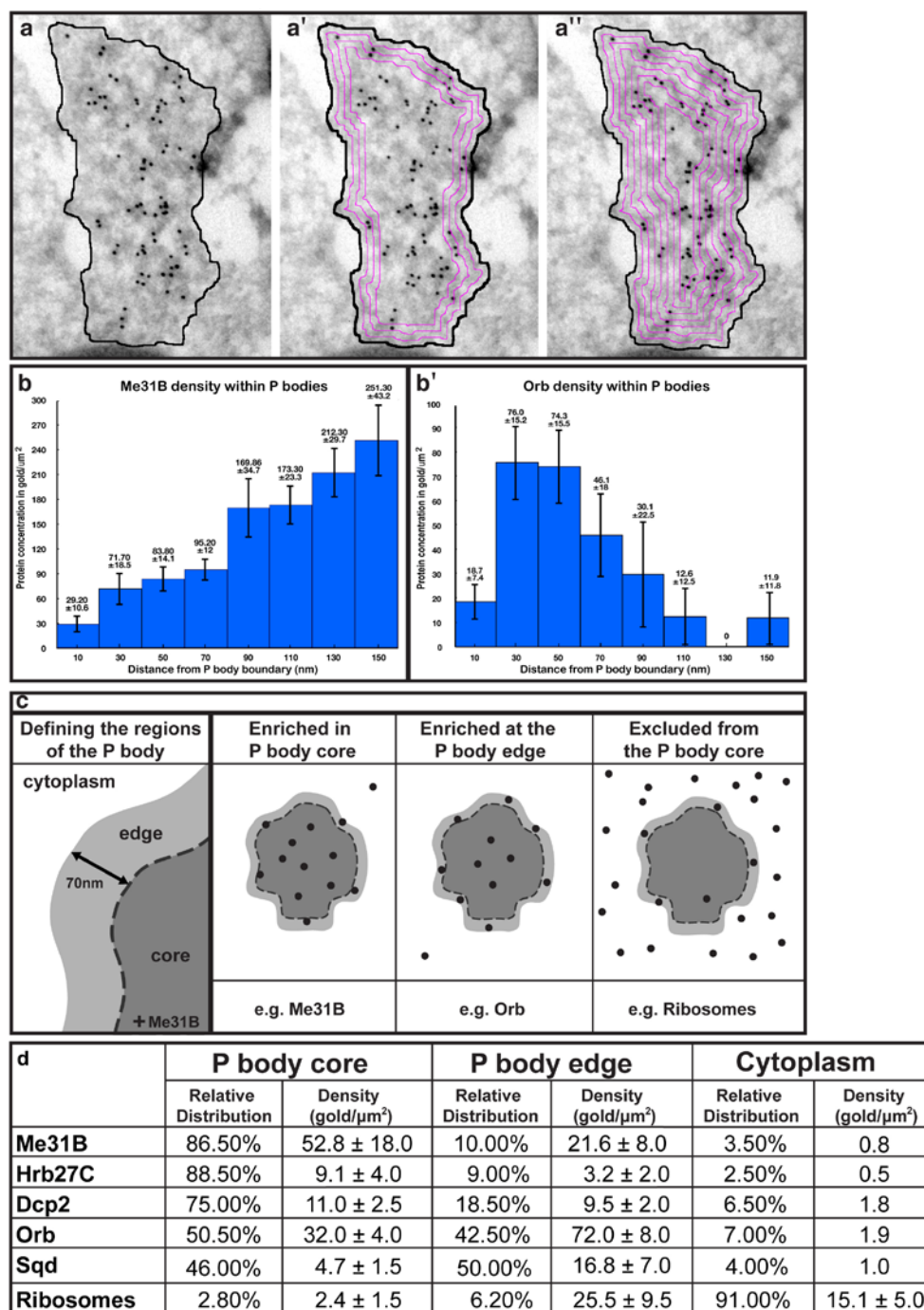


**Figure S2** Definition of P body zones for electron microscopy analysis. (a) A diagram of the objective analysis of P body organization detailed above in 'EM Sample preparation and analysis'. The P body boundary is outlined and concentric regions of interest are added at 20nm increments to 160nm inside of the P body. The area of each 20nm region of interest is calculated and gold particles in each region are counted. (b) Plots of Me31B (and Orb) density versus distance from the P body boundary. SEM: Me31B n=6 scans, Orb n=4 scans. (c) Schematic of P body zones and examples of enriched at the P

body core, enriched at the P body edge and excluded for the P body core are shown. (d) Relative distribution is scored as total number of gold particles compared to gold particles in the P body and in the surrounding cytoplasm. Density is given ± standard deviation: Me31B n=15 scans; Hrb27C n=10 scans; Dcp2 n=8 scans; Orb n=10 scans; Sqd n=12 scans; Ribosomes n=14 scans. For comparative analysis, 'edge' is scored as particles within a 70nm wide region inside the boundary defined by electron density and 'core' is the rest of the P body (See Supplemental Fig. 2c, methods.)

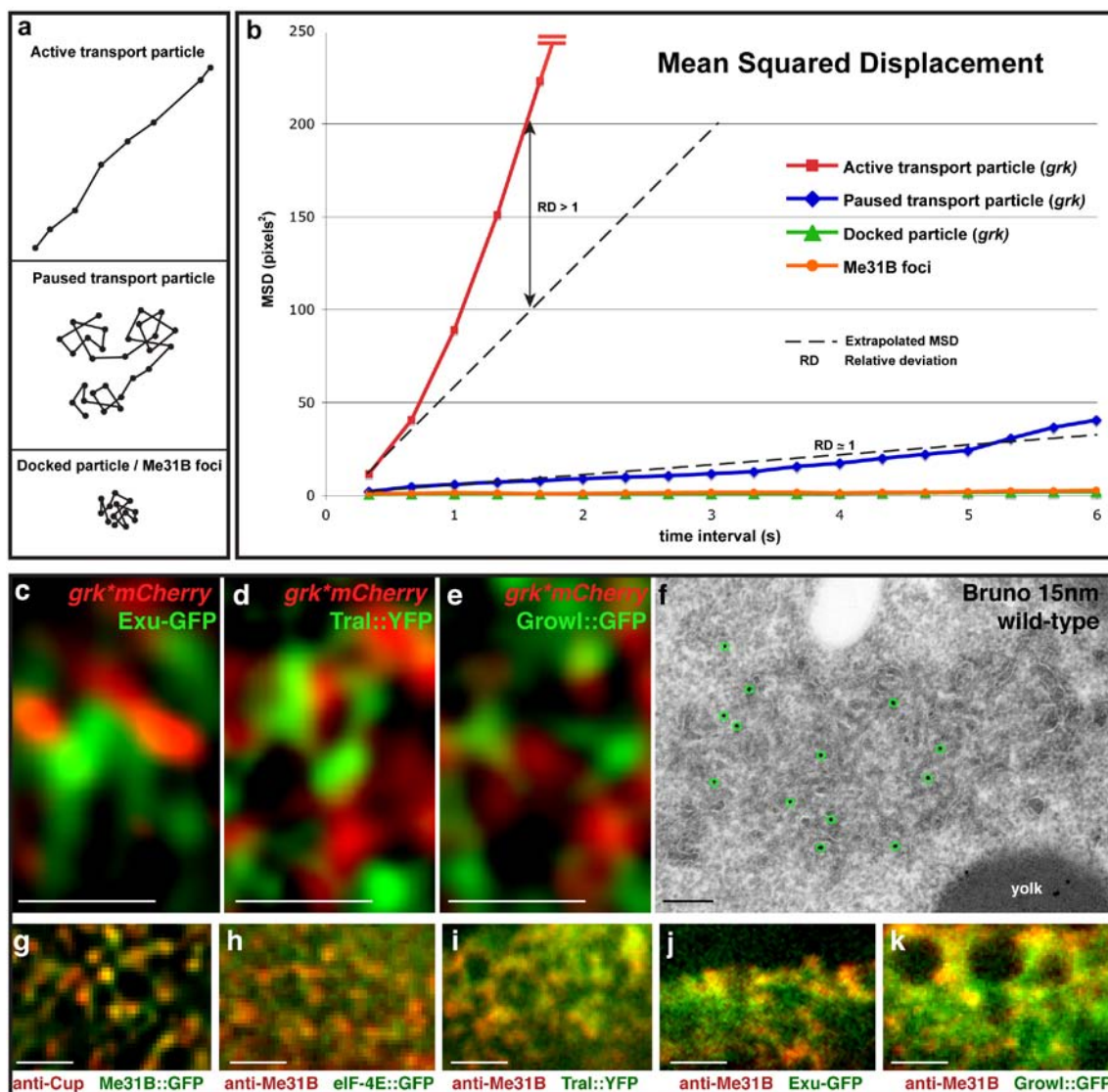


**Figure S3** Formation and distribution of P body components. **(a)** Interpretive diagrams of the three main motion models observed for particles. **(b)** Mean squared displacement plots for a *grk* mRNA active transport particle; *grk* mRNA paused transport particles (average of 8); *grk* mRNA docked particle (average of 5); Me31B::GFP foci (average of 5). Active transport particles shows a MSD characteristic of directed movement (relative deviation (RD) >1) (Supplemental Fig. 3a,b). Paused particles show a complex behavior dominated by slow constrained diffusion (RD = 1), consistent with diffusion in dense cytoplasm<sup>50</sup>, interspersed by short periods of limited motility. In contrast, both docked *grk* mRNA and Me31B foci behave identically and are effectively static, thus suggesting that the two may be physically linked. Furthermore, we observe transitions back and forth between the active transport and paused states. We determine that of the particles not associated with Me31B, 58% of *grk* mRNA particles (Supplementary Movie

1) and 61% of *bcd* mRNA particles are engaged in active transport (n=105) within a 15 second time interval. Taken together, despite having different motion characteristics and transitioning between active and paused states, transport particles are distinct from docked mRNA and Me31B foci. **(c-e)** Wide-field fluorescence and IEM localization of RNA associated proteins in stage 8/9 oocytes expressing *grk*\**mCherry* with **(c)** Exu-GFP or **(d)** Tral::YFP or **(e)** Growl::GFP. *grk* mRNA (red) mainly interdigitates with the proteins (green) while showing some colocalization at the edge (yellow). **(f)** IEM localization of Bruno (15nm, green circles) in a WT egg chamber. **(g-k)** Wide-field fluorescence images of stage 8/9 oocytes expressing **(g)** Me31B::GFP and Cup (red); **(h)** eIF-4E::GFP with labeling for Me31B (red); **(i)** Tral::YFP with labeling for Me31B (red); **(j)** Exu-GFP with labeling for Me31B (red); **(k)** Growl::GFP with labeling for Me31B (red). Scale bars, 0.5µm **(c-e)**; 200nm **(f)**; 2µm **(g-k)**.

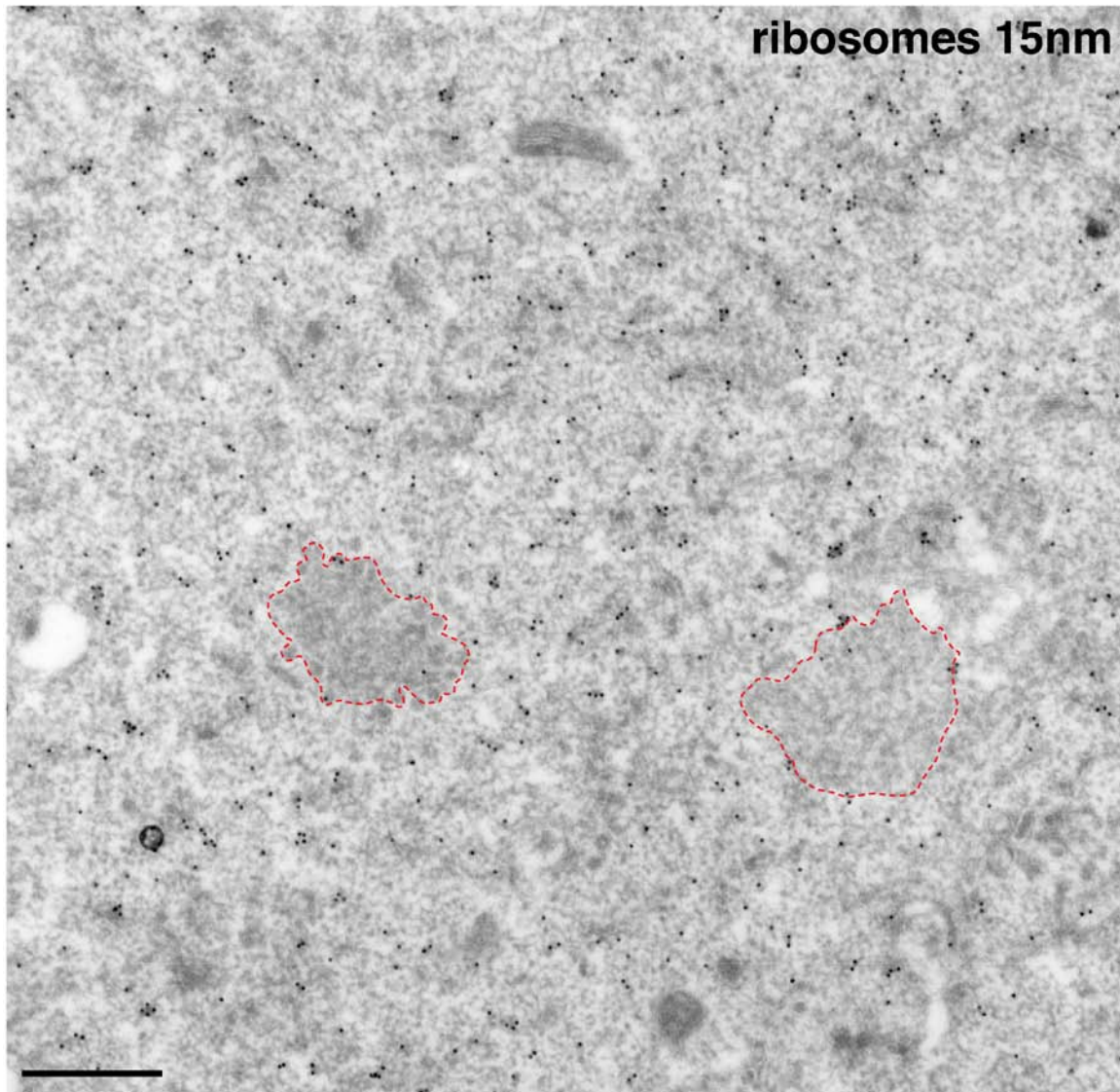


**Figure S4** Ribosomes in relation to P bodies in the oocyte. Low magnification IEM scan of WT oocyte labeled with anti-Ribo 490 identifying ribosomes. P bodies (dashed red line) are virtually devoid of ribosomes inside and show enrichment at the edge. The surrounding cytoplasm is dense with ribosomes. Scale bar, 500nm.

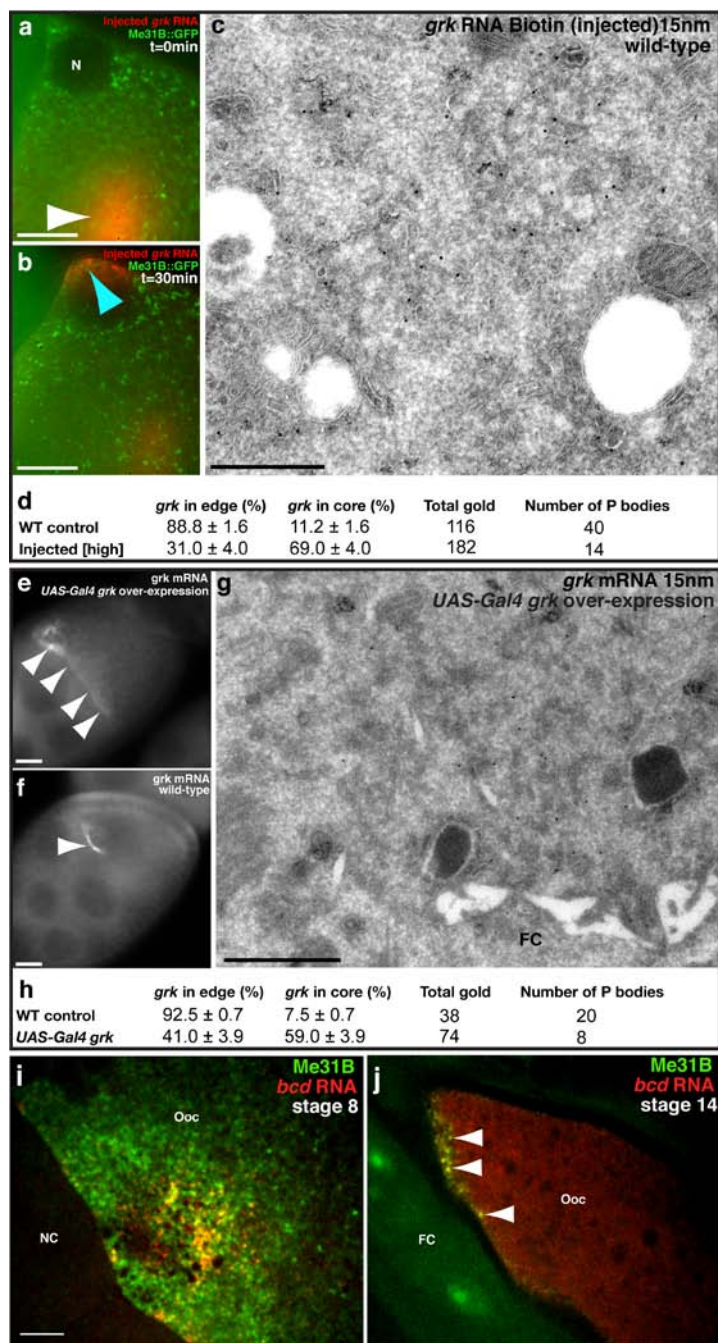


**Figure S5** Differential association of RNA with P bodies. **(a,b)** Me31B::GFP expressing egg chamber **(a)** immediately after injection (white arrowhead) with a moderate concentration of *grk* RNA (120 ng/ $\mu$ l). **(b)** Localized (blue arrowhead), 30 minutes after injection, *grk* RNA is localized to the dorsoanterior corner but does not colocalize with Me31B. **(c)** IEM of a wild-type stage 8/9 egg chamber injected with a high concentration of biotinylated *grk* RNA (500 ng/ $\mu$ l) detected with an anti-Biotin antibody. Injected RNA is detected at the core of and at the edge of P bodies. **(d)** Relative distribution of gold particles labeling *grk* mRNA within P bodies in wild-type and oocytes injected with a high concentration of biotinylated *grk* RNA. Quantitation in the wild-type oocytes is performed using ISH-IEM on endogenous *grk* mRNA. Variation shown as  $\pm$  SEM (wild type n=40; injected n=14). **(e,f)** Fluorescence *in situ* hybridization showing *grk* mRNA distribution (arrowhead) in **(e)** UAS-Gal4 *grk* over-expression and **(f)** wild-type stage 8/9 egg chambers. We

found that, while a majority of mature oocytes showed severe defects in their dorsal appendage, there were some examples with milder phenotypes (11 out of 75). **(g)** ISH-IEM of a UAS-Gal4 *grk* over-expression stage 8/9 oocyte with the highest level of over-expression of *grk*. We observed that P bodies tended to adopt a less compacted morphology, but nevertheless kept their characteristic electron dense material interdigitated with electron light membranous material. **(h)** Relative distribution of *grk* mRNA gold particles within P bodies in wild-type and UAS-Gal4 *grk* over-expression oocytes. Variation shown as  $\pm$  SEM (wild type n=20; UAS-Gal4 *grk* n=8). **(i,j)** Oocytes expressing *bcd*\*RFP and Me31B::GFP showing **(i)** some *bcd* mRNA localized within Me31B rich regions at stage 8 and **(j)** all *bcd* mRNA particles colocalizing with Me31B at stage 14 (white arrowheads). High background autofluorescence is detected in the stage 14 egg chambers. N, nucleus; NC, nurse cell; Ooc, oocyte; FC, follicle cell. Scale bars, 20 $\mu$ m **(a,b,e,f)**; 500nm **(c,g)**; 5 $\mu$ m **(i,j)**.

**Supplementary Movies**

**Movie S1** *grk* mRNA is dynamic in the oocyte. Time lapse movie of the dorsoanterior of an oocyte expressing *grk\*GFP* showing dynamic particles of *grk* mRNA. Images were collected at approximately 3 frames per second and 70 frames are displayed at 15 frames per second.

**Movie S2** Me31B dynamics in the oocyte. Time lapse movie of an oocyte expressing Me31B::GFP showing dynamic particles of Me31B. Small faint dynamic particles move between and fuse together with stationary Me31B bodies. Images were collected at approximately 3 frames per second and 32 frames are displayed at 15 frames per second.

**Movie S3** Me31B dynamics in the oocyte (Low magnification). Time lapse movie of an oocyte expressing Me31B::GFP showing dynamic particles of Me31B. Small faint dynamic particles move between and fuse together with stationary Me31B bodies. Images were collected at approximately 3 frames per second and 35 frames are displayed at 15 frames per second.

**Movie S4** *grk* mRNA moves independently of Me31B. Time lapse movie of an oocyte expressing *grk\*mCherry* and Me31B::GFP showing *grk* mRNA particles moving independently of Me31B. Images were collected simultaneously at approximately 3 frames per second and 17 frames are displayed at 6 frames per second.

**Movie S5** *grk* mRNA docking on Me31B rich bodies. Time lapse movie of an oocyte expressing *grk\*mCherry* and Me31B::GFP showing *grk* mRNA particles docking and remaining on the edge of Me31B rich zones. Merge displayed at the bottom, Me31B top left, *grk* top right. Images were collected simultaneously at approximately 3 frames per second and 33 frames are displayed at 15 frames per second.

**Movie S6** *bcd* mRNA moves independently of Me31B. Time lapse movie of an oocyte expressing *bcd\*RFPP* and Me31B::GFP showing *bcd* particles moving independently of Me31B. Images were collected simultaneously at approximately 3 frames per second and 7 frames are displayed at 6 frames per second.